Low-frequency variability of the North Pacific Ocean: The roles of boundary- and wind-driven baroclinic Rossby waves

Lee-Lueng Fu
Jet Propulsion Laboratory, California Institute of Technology, Pasadena, California, USA

Bo Qiu
Department of Oceanography, University of Hawaii at Manoa, Honolulu, Hawaii, USA

Received 5 September 2001; revised 29 July 2002; accepted 8 August 2002; published 19 December 2002.

[1] The effects of the sea level variability along the eastern boundary of the North Pacific Ocean, including those associated with El Niño Southern Oscillation, have been considered an important factor in determining the low-frequency large-scale variability of the ocean interior through Rossby waves generated at the eastern boundary. This hypothesis is examined in this study using 8 years worth of the sea surface height observations made by the TOPEX/Poseidon satellite. The timescales of interest are longer than 90 days with the annual cycle removed. The results indicate that the influence of the eastern boundary of the North Pacific Ocean has limited offshore extent, varying from 3000–4000 km at 10°N to 200–300 km at 50°N. The variability in the ocean interior is primarily driven by wind with only a minor influence from the boundary. Simulations of a linear two-layer model of the ocean driven by wind stress curl are correlated with the observations. The effects of wind forcing accumulate along the characteristics of long nondispersive Rossby waves in the time-longitude domain. These wind-driven Rossby waves overwhelm the boundary-driven waves in the ocean interior, where there are only some small residual effects of the boundary-driven waves, however. These small effects become clearer after the simulated wind-driven variability is removed from the observations. *INDEX TERMS:* 4556 Oceanography: Physical: Sea level variations; 4504 Oceanography: Physical: Air/sea interactions (0312); 4215 Oceanography: General: Climate and interannual variability (3309); *KEYWORDS:* Rossby waves, satellite altimetry, El Niño, North Pacific, eastern boundary

Citation: Fu, L.-L., and B. Qiu, Low-frequency variability of the North Pacific Ocean: The roles of boundary- and wind-driven baroclinic Rossby waves, *J. Geophys. Res.*, *107*(C12), 3220, doi:10.1029/2001JC001131, 2002.

1. Introduction

[2] El Niño Southern Oscillation (ENSO) events originated in the tropical Pacific have been known to have significant effects on the sea level and circulation of the coastal regions along the coasts of the Americas [*Hurlburt et al.*, 1976; *Johnson and O'Brien*, 1990; *Chelton and Davis*, 1982; *Enfield and Allen*, 1980]. Using a numerical model, *Jacobs et al.* [1994] went one step further and demonstrated how the ENSO effects were able to propagate into the interior Pacific via Rossby waves generated at the eastern boundary of the ocean. They also showed that the differences in the sea surface height of the North Pacific observed in the late 1980s by Geosat and in the early 1990s by ERS-1 could be reproduced by the model simulations and traced to the effects of the 1982–1983 ENSO. They emphasized the importance of the mechanism in relating midlatitude ocean variability to ENSO events generated in the tropics many years earlier and hence in the predictability of the midlatitude climate variations with long lead times. However, there has been little supporting evidence for their hypothesis from more recent and more extensive observations.

[3] Many recent studies [*Miller et al.*, 1997; *Vivier et al.*, 1999; *Qiu*, 2002; *Leonardi et al.*, 2002] suggest that wind forcing by the midlatitude atmosphere is primarily responsible for the low-frequency variability of the interior North Pacific. How well can the Rossby wave signals originated from the eastern boundary be identified in the ocean interior in the presence of the pervasive local wind forcing? Does the local wind forcing overwhelm the remote influence of the boundary in determining the low-frequency variability of the North Pacific? The availability of the continuous, multi-year record of sea surface height collected by the TOPEX/Poseidon (T/P) altimeter provides an opportunity to address these questions. In this study we used the T/P data in the North Pacific covering 1993–2000 to investigate the relationship between the variability of the interior North Pacific and that of the ocean's eastern boundary in terms of

0148-0227/02/2001JC001131$09.00

westward propagating baroclinic Rossby waves. We used a simple linear model to simulate the variability of sea surface height driven by wind and investigated the relative roles of wind forcing versus boundary forcing in the low-frequency variability of the North Pacific Ocean. The term of "wind-forcing" in the paper refers to the local forcing by the midlatitude atmosphere as opposed to the remote forcing by tropical winds for the waves propagating from the ocean boundary. The latter are considered as being forced by the variability along the ocean boundary, and are thus defined as "boundary-driven" waves in the paper.

2. Rossby Wave Dynamics

[4] The wavelengths of Rossby waves at interannual timescales are generally longer than 2000 km [*Chelton and Schlax*, 1996; *Fu and Chelton*, 2001]. They are much longer than the Rossby radius of deformation, which ranges from 80 km to 20 km in the North Pacific from 10°N to 50°N [*Chelton et al.*, 1998]. Therefore the long-wave approximation [*Gill*, 1982] is valid for describing these waves. Following *Qiu* [2002], we use a linear two-layer model for the study. The long-wave equation governing sea surface height, h, is expressed as

$$\frac{\partial h}{\partial t} - \frac{\beta g' H_e}{f^2}\frac{\partial h}{\partial x} = -\frac{g' H_e^2 \nabla \times \tau}{\rho_0 g f H_1^2} - \varepsilon h, \qquad (1)$$

where t is time, x is the longitudinal coordinate (positive eastward), H_1 is the upper layer thickness, H_e is the equivalent depth of the model ($H_e = H_1 H_2/(H_1 + H_2)$), H_2 is the lower layer thickness, ρ_0 is the mean density of sea water, $g' = (\delta\rho/\rho_0)g$ is the reduced gravity ($\delta\rho$ is the density difference between the two layers), f is the Coriolis parameter, β is its meridional gradient, and ε is a Newtonian dissipation rate. Note that there is no y dependence in equation (1). This is because the relative vorticity is negligible when compared to the vortex stretching in the expression of the potential vorticity under the long-wave approximation. The solution to equation (1) can be obtained by integrating along the Rossby wave characteristics in the x-t plane:

$$h(x,t) = h\left(x_e, t - \frac{x - x_e}{c}\right)\exp(-\varepsilon(x - x_e)/c) - \frac{fH_e}{\rho_0 g \beta H_1^2}\int_{x_e}^{x} \nabla \times \tau\left(x', t - \frac{x - x'}{c}\right)\exp(-\varepsilon(x - x')/c)dx' \qquad (2)$$

where

$$c = -\beta g' H_e / f^2, \qquad (3)$$

the phase speed of long baroclinic Rossby waves, x_e is the longitudinal location of the eastern boundary. The first term on the right-hand side of equation (2) represents the influence of the free Rossby waves propagating from the eastern boundary, whereas the second term represents the effects of wind forcing. In order to yield c values close to those of *Killworth et al.* [1997], who took into account the effects of mean flow in computing the Rossby wave phase speed, we set $g' = 0.03\ ms^{-2}$, $H_1 = 246$ m and $H_1 + H_2 = 5000$ m, leading to $H_e = 250$ m. Following *Qiu* [2002], the dissipation rate ε is chosen to be 1/6 year^{-1}. With these parameters, we use equation (2) to simulate the sea surface height in the North Pacific from 10°N to 50°N and investigate the relative roles of the boundary forcing and wind forcing. We begin with the analysis of the variability at the eastern boundary using T/P data.

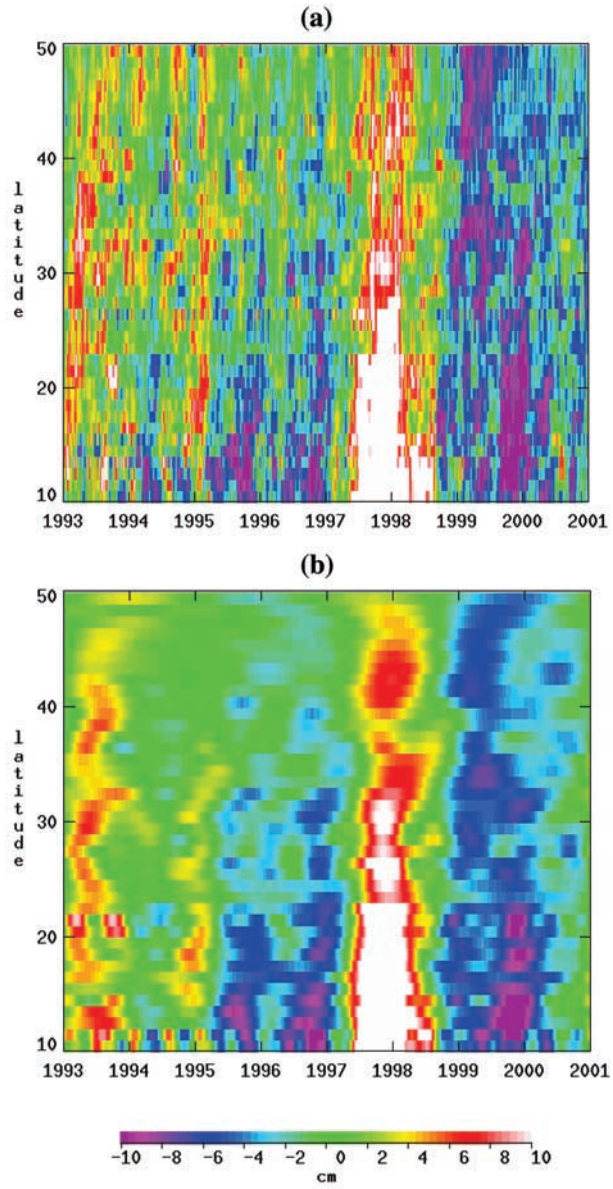

Figure 1. (a) Sea surface height anomalies at the eastern boundary of the North Pacific from latitudes 10°N–50°N. (b) A low-passed version of Figure 1a with frequencies higher than the critical frequency of the first-mode baroclinic Rossby waves removed.

3. Variability at the Eastern Boundary

[5] The T/P data were processed to create a 1° × 1° data set at 3-day intervals. An 8-year mean was first removed at

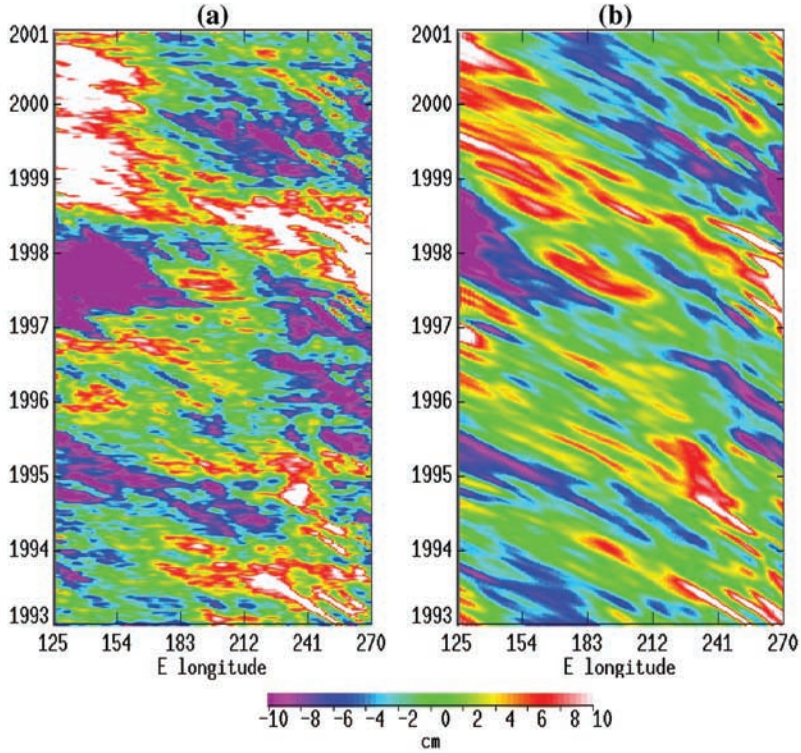

Figure 2. (a) Time-longitude section of the sea surface height anomalies at 10°N. (b) Same as Figure 2a after applying the frequency-wavenumber filtering analysis to extract the Rossby wave signals.

every one-per-second data point along each ground track of the satellite observations. The residuals were averaged in space and time using a Gaussian weighting with scales of 2° in longitude, 1° in latitude, and 5 days in time. Because the annual cycle of the ocean is quite prominent at mid latitudes and it is not of interest to the present study, an annual harmonic was estimated and then removed from the data for the study. This procedure has also removed the steric effects on sea surface height whose timescales are primarily annual [*Stammer*, 1997]. The domain of the study spans 125°E–270°E, 10°N–50°N. The data in the 1° cells closest to the eastern boundary were used for studying the boundary effects. Displayed in Figure 1a is a time-latitude plot of the sea surface height anomalies along the eastern boundary of the ocean. The latitudinally coherent striations of highs and lows are signatures of coastal Kelvin waves propagating northward from the tropics [e.g., *Chelton and Davis*, 1982; *Enfield and Allen*, 1980; *Kessler*, 1990]. The timescales of the variability range from months to years. The signatures of various ENSO events are clearly revealed: the warm events of 1993–1995, followed by a couple of cold events in 1995–1996, culminating with the El Niño of 1997–1998 and ensuing La Niña of 1998–2000. There are a few apparent north-south discontinuities, notably along 23°N where the entrance to the Gulf of California is located. Others are associated with zonally oriented coastlines.

[6] Theoretical studies of the transition of coastally trapped Kelvin waves into Rossby waves that propagate into the ocean interior have suggested the existence of a critical frequency, ω_c [*Clarke*, 1983; *Grimshaw and Allen*, 1988; *Clarke and Shi*, 1991]. For frequencies higher than ω_c, the wave motion is trapped to the boundary as Kelvin waves; for frequencies lower than ω_c, the wave motion is able to propagate away from the boundary as Rossby waves. For a meridional boundary, ω_c is the same as the

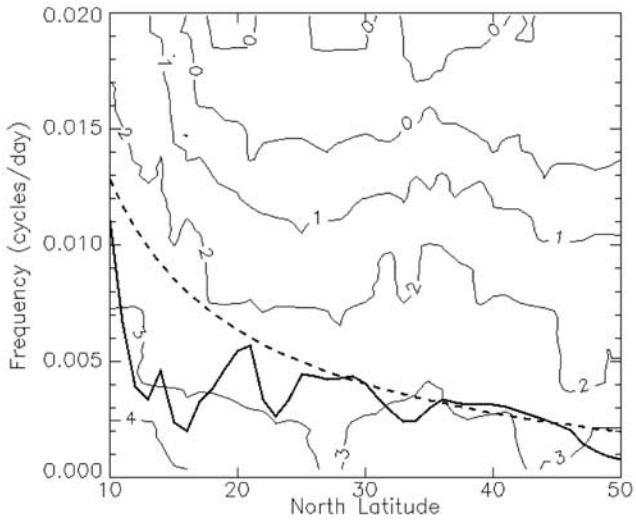

Figure 3. The spectral power density of sea surface height anomalies at 2° in longitude offshore from the eastern boundary of the North Pacific from 10°N–50°N. The contour labels are expressed in terms of $\log_{10}$ of the power density in cm^2/cycle/day. Superimposed are the critical frequencies of Rossby waves obtained from *Clarke and Shi* [1991] (thick solid line) and from equation (4) (dashed line).

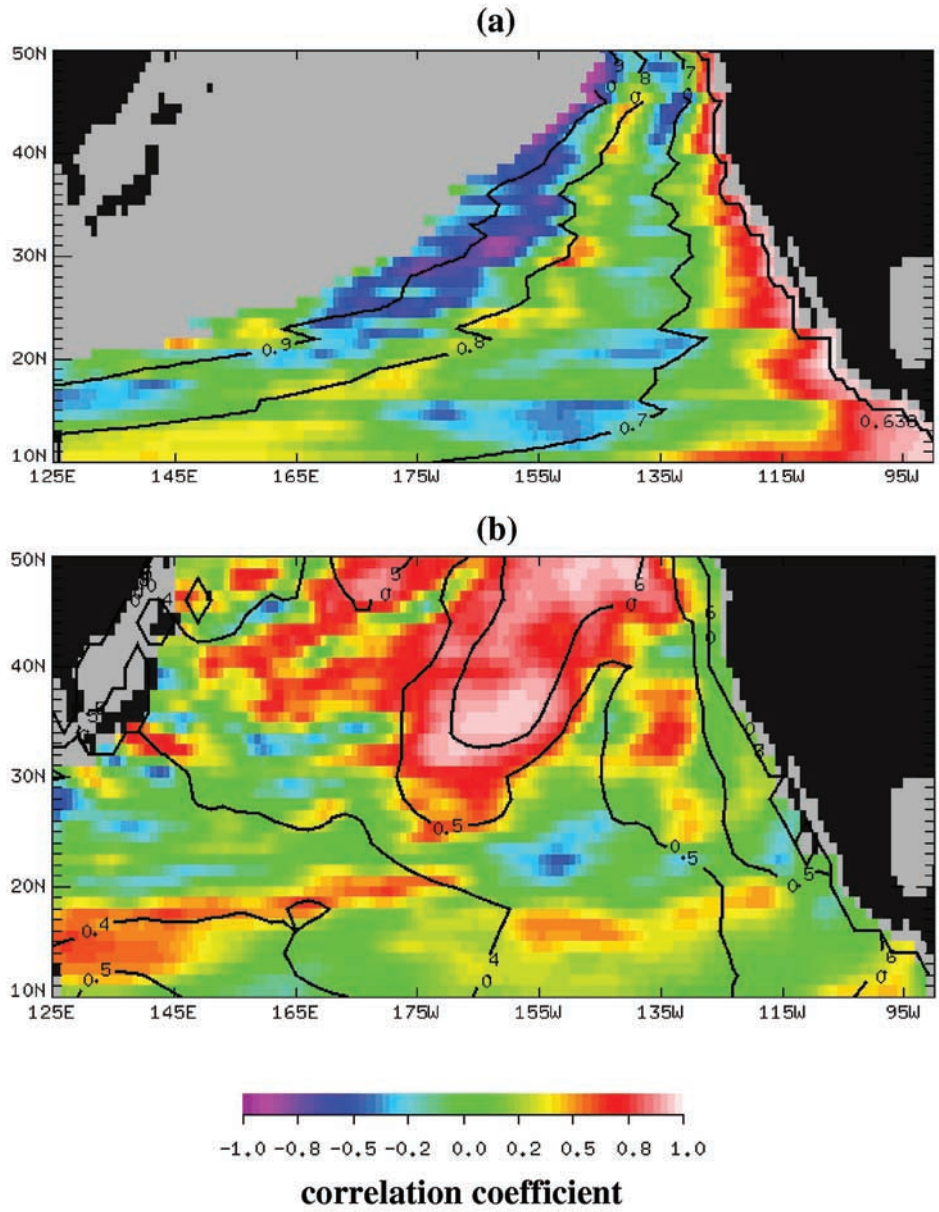

Figure 4. (a) Shown in the color-coded map are the correlation coefficients between the observed sea surface height variability and the variability caused by the boundary-driven Rossby waves. No computation was performed in the gray areas. Contours represent the 95% significance levels for nonzero correlation. (b) Same as Figure 4a except for the correlation coefficients between the observed sea surface height variability and the variability caused by the wind-driven Rossby waves.

maximum frequency for Rossby waves in the open ocean:

$$\omega_c = \frac{\beta c_1}{2f}, \tag{4}$$

where c_1 is the phase speed of the first-mode long gravity waves. The decrease in β and increase in f with latitude make ω_c a decreasing function of latitude. For a nonmeridional boundary, ω_c is modified by the geometry of the coastline, especially the angle between the coastline and the local meridian. When this angle increases, ω_c decreases due to the reduced extent of the meridional movement of the waves to experience the β effect for generating Rossby waves. *Clarke and Shi* [1991] computed the critical frequencies of the first mode Rossby waves for the coastlines of the world's oceans.

[7] To remove the signals that are not able to propagate away from the boundary as Rossby waves, we filtered out the Fourier components that have frequencies higher than ω_c for the west coast of North America obtained from *Clarke and Shi* [1991]. The filtered time series of sea surface height at the eastern boundary is shown in Figure 1b. These low-frequency signals are the source for Rossby waves propagating westward into the ocean interior. Note that the timescales of the filtered signals are increasingly longer at

higher latitudes, where the critical frequencies are generally lower than those at lower latitudes.

[8] To test the frequency dependence of Rossby wave propagation, we examined the frequency spectrum of the westward propagating signals offshore from the eastern boundary. Of interest is whether the westward-propagating signals occur at frequencies lower than the critical values. At a given latitude, we performed zonal wavenumer/frequency Fourier analysis to the two-dimensional array of sea surface height as function of time and longitude. Signals propagating westward were extracted by summing over the westward-propagating Fourier components. The filtered signals were further smoothed over the Rossby wave characteristics in the time-longitude domain to accentuate the Rossby wave signals. Specifically, the smoothed sea surface height, $\bar{h}(x, t)$, is given by $\bar{h} = \frac{1}{N}\Sigma_{i,j}h_{i,j}$, where i, j represent x and t grids satisfying the wave characteristics over a monthly interval. This is essentially a monthly average along the wave characteristics.

[9] Displayed in Figure 2 are the time-longitude plots of sea surface height anomalies along 10°N before and after the application of the filter analysis. The Rossby wave signals stand out after the filtering. The frequency spectra of the filtered signals at 2° of longitude west of the eastern boundary are shown in Figure 3. This represents the energy of Rossby waves primarily generated by the coastal variability shown in Figure 1. Superimposed on Figure 3 are the critical frequencies based on equation (4) as well as on the values of *Clarke and Shi* [1991]. The phase speeds of the first-mode long gravity waves, c_1 in equation (4), were obtained from *Chelton et al.* [1998]. The distribution of the bulk of the wave energy is indeed at frequencies lower than the critical values. The energy at frequencies higher than the critical values is about an order of magnitude smaller than that at lower frequencies, demonstrating the concept of the critical frequency of Rossby waves. Note that in Figure 3 the contour corresponding to 10^3 cm^2/cycle/day basically follows the thick solid line representing the critical frequencies obtained from *Clarke and Shi* [1991].

4. Boundary-Driven Waves

[10] The sea surface height at the eastern boundary (Figure 1b) was used to compute the first term on the right-hand side of equation (2) to simulate the boundary-driven Rossby waves. The values of c based on the standard theory of Rossby waves represented by equation (3) were obtained from *Chelton et al.* [1998] on a $1° \times 1°$ grid. We then adjusted the values to account for the effects of an east-west mean flow according to the computation of *Killworth et al.* [1997]. The adjustment was made at each latitude based on the ratio of the speed from Killworth et al. to the speed from the standard theory. We computed the correlation coefficients between the simulation and the 8-year T/P data. Because the highest critical Rossby-wave frequency in the domain of study is about 0.011 cycles/day (90 day period; see Figure 3), the T/P data were smoothed by a 90-day running averaging to filter out the high-frequency variability. This averaging has removed most of the barotropic signals whose timescales are generally less than 100 days [*Fukumori et al.*, 1998]. There are also barotropic signals at seasonal scales [*Vivier et al.*, 1999; *Qiu*, 2002], but they have also been removed as part of the annual cycle. The results of the correlation analysis are shown in Figure 4a.

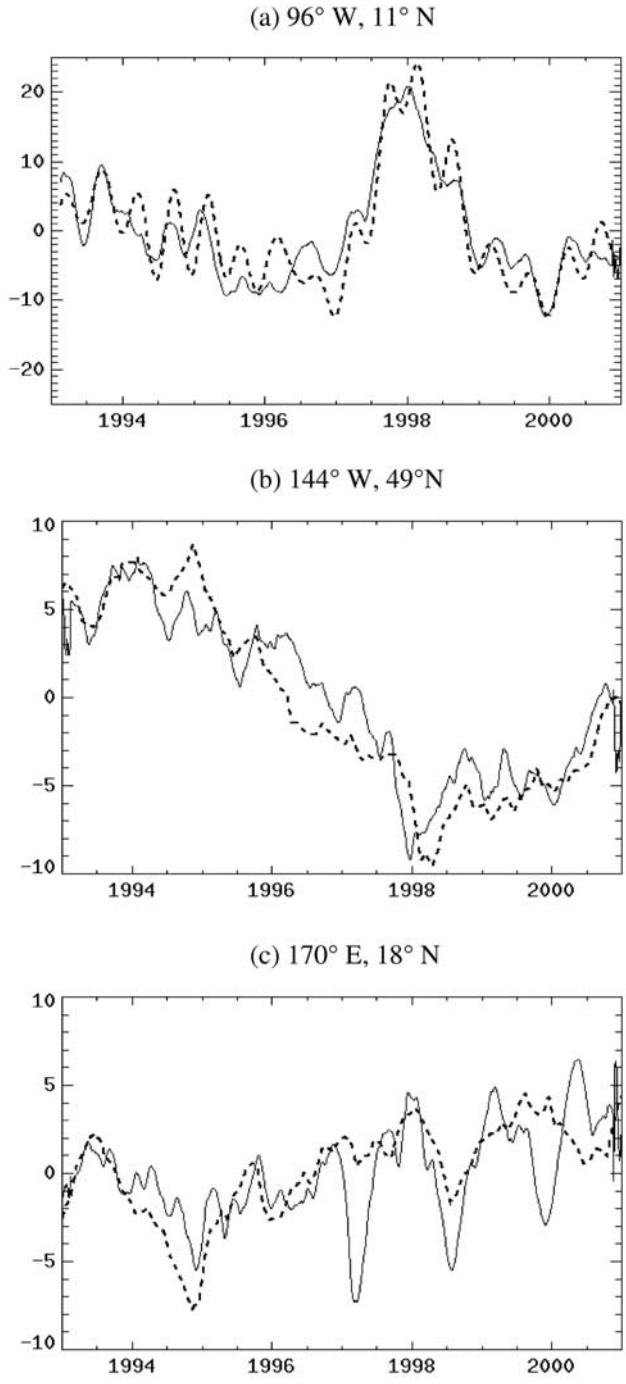

Figure 5. Time series of sea surface height anomalies at three locations: (a) 96°W, 11°N; (b) 144°W, 49°N; (c) 170°E, 18°N. Solid lines are T/P observations. Dashed lines are boundary-driven anomalies in Figure 5a and wind-driven anomalies in Figures 5b and 5c.

[11] The lack of results in the northwest part of the basin is attributed to the slowness of the wave speed, varying from 20 cm/s at 10°N to 1 cm/s at 50°N. Depending on

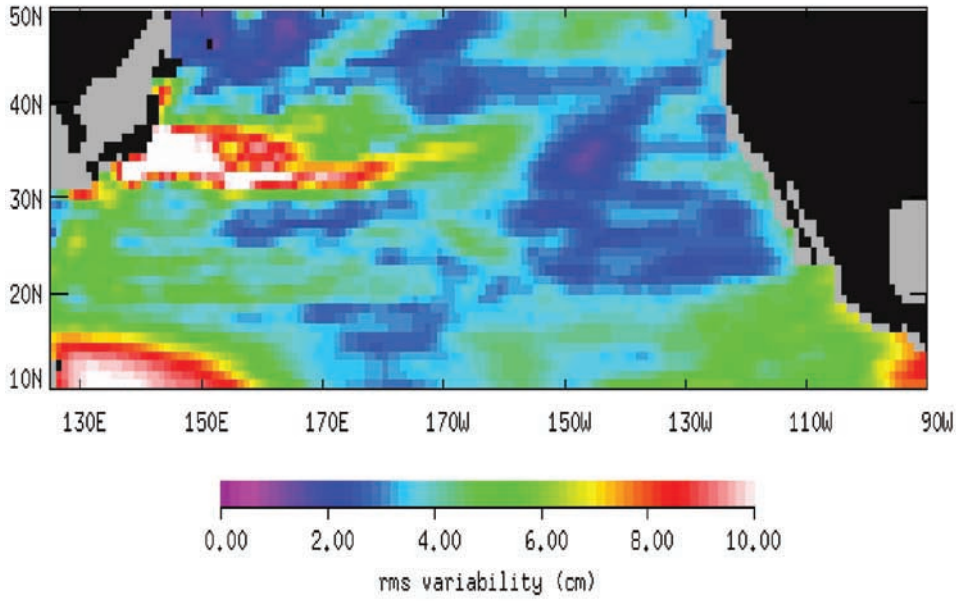

Figure 6. Root-mean-squares variability of the 90-day smoothed sea surface height variability in cm (with the annual cycle removed).

latitude, it takes 2–20 years for the waves to travel across the ocean basin. Because of insufficient record length, none of the waves started at the eastern boundary since the beginning of the record in 1993 have the time to reach the northwestern part of the basin. Furthermore, we require at least 1200 days worth of data for computing the correlation with the observations. Next to the northwestern limit where the waves have just reached, the data length is too short to be included in the analysis. Therefore the area in which the correlation is displayed is even smaller than that reached by the boundary-driven waves.

[12] The timescales of the boundary-driven waves, estimated from the integral of the temporal autocorrelation function of the variability [*Richman et al.*, 1977], are about 300 days. The number of degrees of freedom for the correlation estimate is determined by dividing the record length by this timescale. The 95% significance level for nonzero correlation is about 0.64 near the eastern boundary where the time series is the longest, and increases to 0.95 near the western border of the domain of the correlation analysis. Significant correlation occurs only near the eastern boundary. Note that the offshore edge of significant correlation reflects the shape of the coastline, consistent with the transmission of the influence of the boundary via wave propagation.

[13] Shown in Figure 5a is comparison of the simulation with the observation at 96°W, 11°N, where the correlation is significant. The agreement between the simulation and the observation indicates that the 1997–1998 El Niño created a boundary-driven wave that traveled to this location. It takes only 55 days for a Rossby wave to arrive at the location, which is 700 km offshore. At 11°N, the critical Rossby wave frequency is 0.011 cycle/day (90-day period; see the thick solid line in Figure 3), which is sufficiently high to allow the propagation of intraseasonal coastal Kelvin waves into open ocean Rossby waves. These intraseasonal coastal variability is visible in Figure 1, particularly near the bottom of Figure 1b.

[14] As indicated in Figure 4a, the correlation coefficients in the ocean interior are mostly insignificant. This implies that the wind-driven variability might dominate in the ocean interior, or that the boundary-driven waves cannot be described by equation (1) once they have left the coastal region. In fact, the former does not necessarily rule out the latter. Also of interest is the presence of the band of a secondary maximum of correlation in the ocean interior, stretching from 45°N, 140°W to 10°N, 125°W. We will come back to this point later after the discussion of the wind-driven waves.

5. Wind-Driven Waves

[15] Monthly wind stress curl computed from the reanalysis wind products of the National Center of Environmental Prediction (NCEP) [*Kalnay et al.*, 1996] was used to compute the wind-driven variability represented by the second term on the right-hand side of equation (2). The values of c were also adjusted for consistency with *Killworth et al.* [1997]. The time span of the wind data begins in 1980 to ensure the coverage of all the wave characteristics for the entire domain of study during 1993–2000. The correlation between the simulation and the T/P observation is shown in Figure 4b. The 95% significance level for nonzero correlation was computed from the degrees of freedom based on the integral timescales [*Richman et al.*, 1977] estimated from the T/P observations. In the areas of significant correlation, the sea surface height is coherent with the simulations derived from the wind-driven solution to equation (1).

[16] The areas of significant correlation are primarily in the ocean interior north of 30°N. These areas correspond fairly well to the regions of significant sea-surface-height

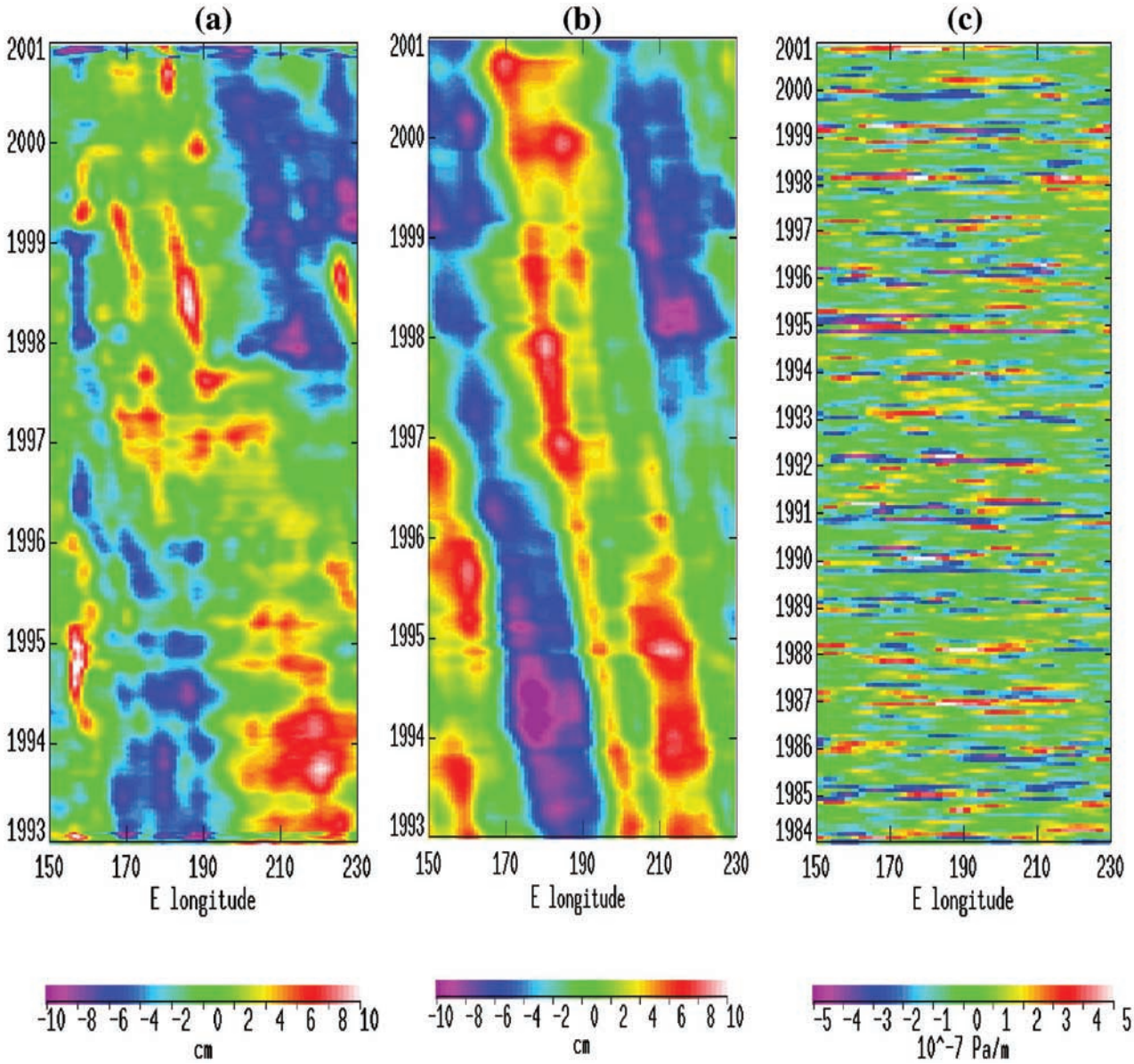

Figure 7. Time longitude plots along 49°N: (a) Sea surface height anomalies (in cm) from the T/P observation. (b) Sea surface height anomalies (in cm) from the simulated wind-driven Rossby waves. (c) The wind stress curl anomalies (in 10^{-7} Pa/m) used to drive the sea surface height anomalies shown in the middle panel. Note the timescale for Figure 7c is different from those for Figures 7a and 7b.

variability (the green/yellow/red areas in Figure 6) except for the region of the Kuroshio, where the variability is dominated by mesoscale eddies not described by equation (1). South of 20°N, there are two long and narrow regions with significant correlation (one from 125°E to 175°W; the other from 155°W to 115°W). These two regions also correspond to regions of high (western region) and moderate (eastern region) variability outside the zone of boundary influence (see Figure 4a). The correlation is generally below significance level within 20°N–30°N. In this region the variability to the east of 150°W is very low and approaches the noise level (2 cm in the blue areas). To the west of 150°W, the moderate variability (4–6 cm) is primarily due to the mesoscale eddies associated with the subtropical countercurrent [*Qiu*, 1999] and cannot be accounted for by the wind-driven variability. The causes for some of the low-correlation areas are also associated with the overly simplistic Rossby wave characteristics considered in the study. As shown by *de Szoeke* [1995], actual Rossby wave characteristics are perturbed by the background mean flow, which might lead to a meridional component in the wave propagation. Such aspects are beyond the scope of the present study.

[17] The results of the correlation analysis suggest that the low-frequency variability in the ocean interior away from the areas of strong mesoscale variability is largely due to wind forcing. Details of the temporal variability are examined in a couple of locations. Comparison of the simulated wind-driven variability with the T/P observation at 144°W, 49°N is shown in Figure 5b. The variability is

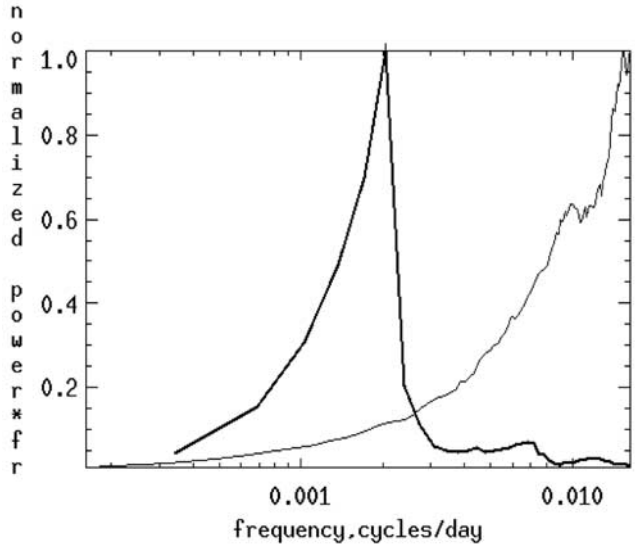

Figure 8. Zonally averaged variance-preserving spectra of the wind stress curl (thin line) and the wind-driven sea surface height anomalies (thick line) along 49°N. The spectra are normalized by their respective maximum values.

dominated by a timescale comparable to the 8-year record length. As stated by equation (2), the wind-driven variability at a given location and time results from the wind forcing to the east and prior in time according to the characteristics of Rossby waves. Because the Rossby wave speed is much lower at high latitudes than at low latitudes, the wind-driven variability at high latitudes results from a longer integration of past wind events than at low latitudes. The timescales of the wind-driven variability are thus shorter at lower latitudes (see Figure 5c for a location at 170°E, 18°N). However, the energetic fluctuations at this location on timescales shorter than one year are not reproduced by the simulation. They may be governed by nonlinear mechanisms of eddy formation in the region [*Qiu*, 1999].

[18] Shown in Figures 7a and 7b is comparison of time-longitude sections along 49°N from the T/P observation and the simulated wind-driven variability. As indicated by the correlation shown in Figure 4b, the simulation has captured most of the observed features. The westward phase propagation of the simulated variability is quite persistent at interannual timescales. However, the timescales of the wind forcing (Figure 7c) are much shorter. Shown in Figure 8 are the zonally averaged variance-preserving spectra (power density multiplied by frequency) of the wind stress curl and the simulated sea surface height at 49°N. The bulk of the energy of wind stress curl resides at timescales less than a year, while the bulk of the sea surface height energy resides at the interannual scales. The Rossby waves serve like an integrator that low-passes the wind variability in forcing the ocean. The agreement between the simulation and the observation suggests that the interannual variability of the sea surface height is forced by wind in a manner similar to the phenomenon of random walk. In fact the solution represented by equation (2) essentially describes a random walk response of the ocean to wind forcing along the characteristics of Rossby waves in the time-longitude domain. The concept of generating low-frequency variability by stochastic forcing has been demonstrated by theoret-

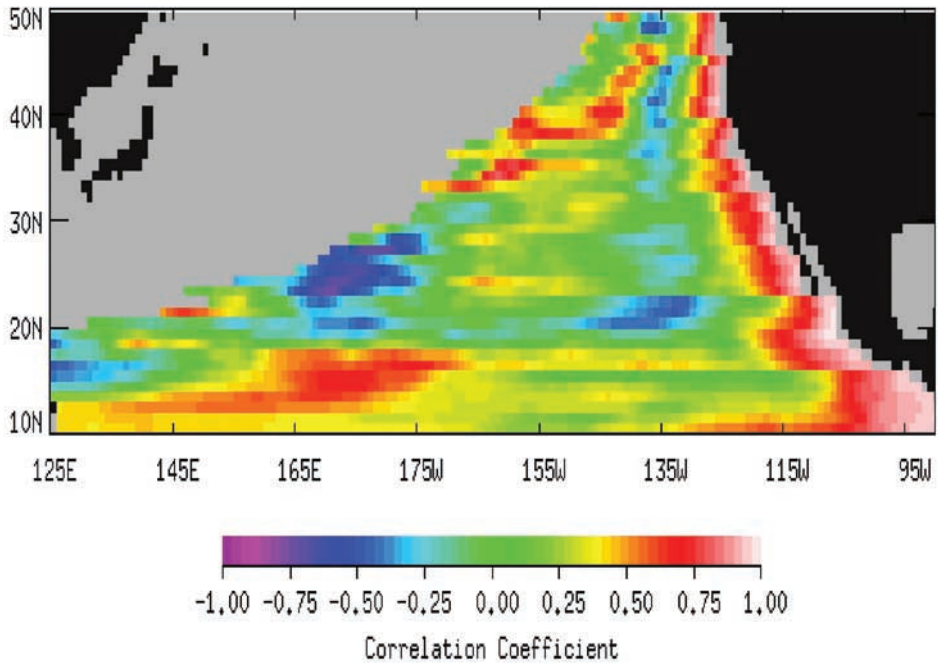

Figure 9. Correlation coefficients between the variability caused by the boundary-driven Rossby waves and the observed sea surface height variability after the wind-driven variability is removed from the observations.

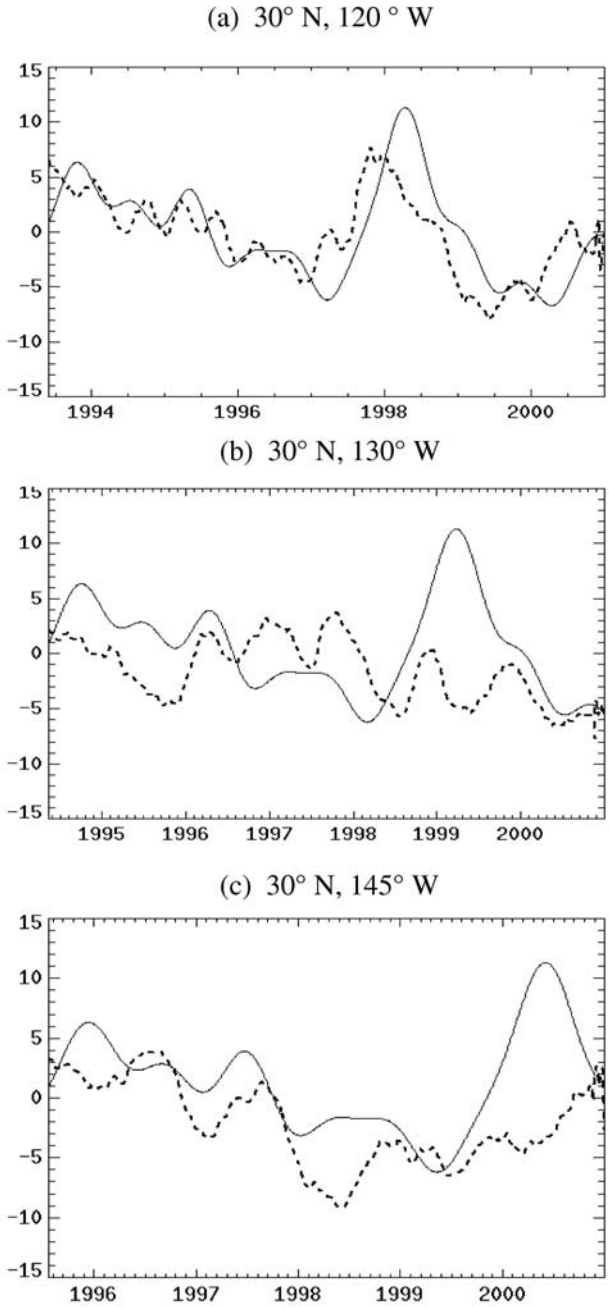

Figure 10. Sea surface height time series along 30°N at various longitudes: (a) 120°W, (b) 130°W, (c) 145°W. The solid lines represent the boundary-driven waves derived from equation (2). The dashed lines represent the observations with the wind-driven waves derived from equation (2) removed.

ical studies [e.g., *Frankingnoul et al.*, 1997]. The present study has provided observational evidence for this mechanism in the North Pacific Ocean.

6. Residual Effects of the Boundary-Driven Waves in the Ocean Interior

[19] As noted in section 4, there is a secondary band of high correlation between the boundary-driven waves and the observed variability in the ocean interior. This band happens to lie in the regions of significant correlation between the observations and the wind-driven variability. The dominance of wind forcing might have masked the effects of the boundary-driven waves. To remove the wind effects for examining the boundary effects, we subtracted the simulated wind-driven variability from the observations and computed the correlation between the difference and the boundary-driven variability (the first term on the right-hand side of equation (2)). The result is shown in Figure 9. The correlation in the ocean interior is generally higher than the previous estimate (Figure 4a), although still not statistically significant. Note especially that the area of negative correlation to the west of the secondary high correlation band in Figure 4a is much reduced.

[20] The sharp offshore decrease in the correlation coefficient is still present in Figure 9, indicating that the boundary-driven waves cannot be described by the solution to equation (1). The wave dispersion (including meridional propagation) and dissipation processes that are not included in our simple model might become important offshore. These waves apparently become dispersive after leaving the coast. Note the breakup of the wave associated with the 1997–1998 El Niño at 30°N, 130°W shown in Figure 10b. However, the long-wavelength components of a dispersed wave group, propagating at a speed close to the nondispersive wave speed, are the fastest among all the wave components. The trailing short-wavelength components dissipate rapidly due to their smaller spatial scales. Such dissipation is not included in our simple model, but can be readily included in a standard Laplacian dissipation scheme in a more complicated model. Scales close to the internal Rossby radius of deformation are more susceptible to dissipation than larger scales. At certain distance from the boundary, only the long-wavelength components of the boundary-driven waves remain and they regain some correlation with the solution to equation (1) (Figure 10c). Also note that the shape of the band is consistent with a nondispersive, low-frequency Rossby wave front resulting from the latitudinally varying wave speed [*Chelton and Schlax*, 1996]. Therefore the scenario described above is a plausible explanation for the secondary band of high correlation in the ocean interior.

7. Conclusions

[21] The analysis of 8-year record of sea surface height observations made by TOPEX/Poseidon has shown a rather limited influence of boundary-driven Rossby waves on the low-frequency variability of the interior North Pacific. Sea surface height observations along the west coast of North America were filtered to retain only the signals that have frequencies lower than the critical frequency of Rossby waves. These signals were projected onto nondispersive Rossby waves that were subsequently allowed to propagate westward into the ocean interior. Extensive offshore influence by these boundary-driven waves is seen only at the tropical latitudes. Significant correlation between the observed sea surface height variability and the simulated wave signals is confined to regions adjacent to the coast with an offshore extent varying from 3000–4000 km at 10°N to 200–300 km at 50°N.

[22] The rapid degradation of the correlation offshore may be caused by the dispersion of the waves not allowed in the nondispersive wave model. After the trailing short-wavelength components of the dispersed waves have dissipated, the remaining long-wavelength components then follow the nondispersive model. This scenario provides a plausible explanation for the secondary band of high correlation in the ocean interior, as well as its shape of a nondispersive Rossby wave front. Although the secondary correlation is not statistically significant, its large-scale spatial pattern suggests that some residual effects of the boundary-driven waves do exist in the ocean interior. After the wind-driven variability is removed from the observations, the residual effects become even clearer.

[23] Using a linear two-layer model with long-wave approximation, we simulated the wind-driven variability of sea surface height and compared it to the observations. The wind stress curl was obtained from the monthly NCEP reanalysis product. Significant correlation between the observation and simulation is found in the open ocean away from the limited areas of strong mesoscale variability, suggesting that wind is the dominant forcing of the observed variability in most of the ocean interior. The boundary influence related to past ENSO events suggested by *Jacobs et al.* [1994] is masked by the prevailing wind forcing and thus plays only a secondary role in the low-frequency variability of the North Pacific.

[24] The influence of the wind accumulates along the characteristics of Rossby waves in the time-longitude domain. Through integration in time and space, only the low-frequency components of the wind variability are important in forcing the ocean. *Sturges and Hong* [1995] and *Hong et al.* [2000] demonstrated that the wind forcing was responsible for the sea level variability at Bermuda and the U.S. east coast on decadal scales. *Lagerloef* [1995] suggested that the decadal variability of the Alaska gyre was forced by stochastic wind events. The present study provides evidence suggesting stochastic wind forcing as an effective mechanism for low-frequency variability in a large area of the North Pacific.

[25] **Acknowledgments.** We are grateful to Dudley Chelton of the Oregon State University for his review and comments on an earlier version. John Toole provided invaluable editorial assistance. The research presented in the paper was partly carried out by the Jet Propulsion Laboratory, California Institute of Technology, under contract with the National Aeronautic and Space Administration. Support from the TOPEX/POSEIDON Project and Jason-1 is acknowledged. The effort of Bo Qiu was supported by the Jason-1 Project through contract 1207881 issued to the University of Hawaii.

References

Chelton, D. B., and R. E. Davis, Monthly mean sea level variability along the west coast of North America, *J. Phys. Oceanogr.*, *12*, 757–784, 1982.

Chelton, D. B., and M. G. Schlax, Global observations of oceanic Rossby waves, *Science*, *272*, 234–238, 1996.

Chelton, D. B., R. A. de Szoeke, M. G. Schlax, K. E. Naggar, and N. Siwertz, Geographical variability of the first baroclinic Rossby radius of deformation, *J. Phys. Oceanogr.*, *28*, 433–460, 1998.

Clarke, A. J., The reflection of equatorial waves from oceanic boundaries, *J. Phys. Oceanogr.*, *13*, 1193–1207, 1983.

Clarke, A. J., and C. Shi, Critical frequencies at ocean boundaries, *J. Geophys. Res.*, *96*, 10,731–10,738, 1991.

de Szoeke, R., A model of wind- and buoyancy-driven ocean circulation, *J. Phys. Oceanogr.*, *25*, 918–941, 1995.

Enfield, D. B., and J. S. Allen, On the structure and dynamics of monthly mean sea level anomalies along the Pacific coast of North and South America, *J. Phys. Oceanogr.*, *10*, 557–578, 1980.

Frankingnoul, C., P. Muller, and E. Zorita, A simple model of the decadal response of the ocean to stochastic wind forcing, *J. Phys. Oceanogr.*, *27*, 1533–1546, 1997.

Fu, L.-L. and D. B. Chelton, Large-scale ocean circulation and variability, in *Satellite Altimetry and Earth Sciences*, edited by L.-L. Fu and A. Cazenave, pp. 133–169, Academic, San Diego, Calif., 2001.

Fukumori, I., R. Raghunath, and L.-L. Fu, The nature of global large-scale sea level variability in relation to atmospheric forcing: A modeling study, *J. Geophys. Res.*, *103*, 5493–5512, 1998.

Gill, A. E., *Atmosphere-Ocean Dynamics*, 662 pp., Academic, San Diego, Calif., 1982.

Grimshaw, R., and J. S. Allen, Low-frequency baroclinic waves off coastal boundaries, *J. Phys. Oceanogr.*, *18*, 1124–1143, 1988.

Hong, B. G., W. Sturges, and A. J. Clarke, Sea level on the U.S. east coast: decadal variability caused by open ocean wind-curl forcing, *J. Phys. Oceanogr.*, *30*, 2088–2098, 2000.

Hurlburt, H. E., J. C. Kindle, and J. J. O'Brien, A numerical simulation of the onset of El Niño, *J. Phys. Oceanogr.*, *6*, 621–631, 1976.

Jacobs, G. A., H. E. Hurlburt, J. C. Kindle, E. J. Metzger, J. L. Mitchell, W. J. Teague, and A. J. Wallcraft, Decade-scale trans-Pacific propagation and warming effects of an El Niño anomaly, *Nature*, *370*, 360–363, 1994.

Johnson, M. A., and J. J. O'Brien, The northeast Pacific Ocean response to the 1982–1983 El Niño, *J. Geophys. Res.*, *95*, 7155–7166, 1990.

Kalnay, E., et al., The NCEP/NCAR 40-year reanalysis project, *Bull. Am. Meteorol. Soc.*, *77*, 437–471, 1996.

Kessler, W. S., Observations of long Rossby waves in the northern tropical Pacific, *J. Geophys. Res.*, *95*, 5183–5217, 1990.

Killworth, P. D., D. B. Chelton, and R. A. De Szoeke, The speed of observed and theoretical long extra-tropical planetary waves, *J. Phys. Oceanogr.*, *27*, 1946–1966, 1997.

Lagerloef, G., Interdecadal variations in the Alaska Gyre, *J. Phys. Oceanogr.*, *25*, 2242–2258, 1995.

Leonardi, A. P., S. L. Morey, and J. J. O'Brien, Interannual variability in the eastern North Pacific Ocean, *J. Phys. Oceanogr.*, *32*, 1824–1837, 2002.

Miller, A. J., W. B. White, and D. R. Canyan, North Pacific thermocline variations on ENSO timescales, *J. Phys. Oceanogr.*, *27*, 2023–2039, 1997.

Qiu, B., Seasonal eddy field modulation of the North Pacific subtropical countercurrent: TOPEX/POSEIDON observations and theory, *J. Phys. Oceanogr.*, *29*, 2471–2486, 1999.

Qiu, B., Large-scale variability in the mid-latitude subtropical and subpolar North Pacific Ocean: Observations and causes, *J. Phys. Oceangr.*, *32*, 353–375, 2002.

Richman, J. G., C. Wunsch, and N. G. Hogg, Space and timescales of mesoscale motion in the western North Atlantic, *Rev. Geophys. Space Phys.*, *15*, 385–420, 1977.

Stammer, D., Steric and wind-induced changes in TOPEX/POSEIDON large-scale sea surface topography observations, *J. Geophys. Res.*, *102*, 20,987–21,009, 1997.

Sturges, W., and B. G. Hong, Wind forcing of the Atlantic thermocline along 32N at low frequencies, *J. Phys. Oceanogr.*, *25*, 1706–1715, 1995.

Vivier, F., K. A. Kelly, and L. Thompson, Contributions of wind forcing, waves, and surface heating to sea-surface height observations in the Pacific Ocean, *J. Geophys. Res.*, *104*, 20,767–20,788, 1999.

L.-L. Fu, Jet Propulsion Laboratory, California Institute of Technology, Pasadena, CA 91109, USA. (llf@pacific.jpl.nasa.gov)

B. Qiu, Department of Oceanography, University of Hawaii at Manoa, 1000 Pope Road, Honolulu, HI 96822, USA. (bo@soest.hawaii.edu)